

NEW CANDIDATES FOR PLANETARY-MASS BROWN DWARFS IN IC 348

K. L. LUHMAN^{1,2} AND C. J. HAPICH¹

Draft version June 11, 2020

ABSTRACT

We have used infrared images obtained with the Wide Field Camera 3 on board the *Hubble Space Telescope* to search for planetary-mass brown dwarfs in the star-forming cluster IC 348. In those images, we have identified 12 objects that have colors indicative of spectral types later than M8, corresponding to masses of $\lesssim 30 M_{\text{Jup}}$ at the age of IC 348. The four brightest candidates have been observed with spectroscopy, all of which are confirmed to have late types. Two of those candidates appear to be young, and thus are likely members of the cluster, while the ages and membership of the other two candidates are uncertain. One of the former candidates is the faintest known member of IC 348 in extinction-corrected K_s and is expected to have a mass of 4–5 M_{Jup} based on evolutionary models and an assumed age of 3 Myr. Four of the remaining eight candidates have ground-based photometry that further supports their candidacy as brown dwarfs, some of which are fainter (and potentially less massive) than the known members.

1. INTRODUCTION

Over the last decade, searches for free-floating brown dwarfs have reached progressively deeper into the mass regime of planetary companions ($\lesssim 15 M_{\text{Jup}}$) in the solar neighborhood (Cushing et al. 2011; Luhman 2014; Kirkpatrick et al. 2019; Bardalez Gagliuffi et al. 2020; Meisner et al. 2020) and in the nearest young associations (Liu et al. 2013; Kellogg et al. 2015; Burgasser et al. 2016; Schneider et al. 2016; Best et al. 2017; Gagné et al. 2018) and star-forming regions (Scholz et al. 2012; Esplin et al. 2017; Zapatero Osorio et al. 2017; Lodieu et al. 2018; Esplin & Luhman 2019; Robberto et al. 2020). The IC 348 cluster in the Perseus molecular cloud (Herbst 2008) has been one of the most thoroughly surveyed examples of the latter because of several characteristics: young enough that its brown dwarfs are relatively luminous (2–6 Myr, Luhman et al. 2003; Bell et al. 2013); old enough that most of its members are not heavily obscured ($A_V < 3$); among the nearest star-forming clusters (~ 300 pc); sufficiently well-populated to provide good statistical constraints on the substellar mass function ($N \sim 500$); compact enough to allow efficient imaging (~ 0.2 deg²); and relatively low nebular emission because of the absence of an H II region. The latest census of IC 348 contains 67 objects likely to be brown dwarfs ($\geq M6.5$), has a high level of completeness down to $\sim 10 M_{\text{Jup}}$ ($\sim 0.01 M_{\odot}$), and reaches masses as low as $\sim 5 M_{\text{Jup}}$ (Alves de Oliveira et al. 2013; Luhman et al. 2016; Esplin & Luhman 2017, references therein).

Brown dwarfs are typically identified using photometry or proper motions measured from wide-field surveys or deep imaging of small fields toward young clusters. Standard broad-band filters at optical and infrared (IR) wavelengths have been successfully utilized in the photometric selection process, but filters that are

designed to measure absorption bands from H₂O and CH₄ produce particularly distinctive colors for brown dwarfs (Najita et al. 2000; Mainzer & McLean 2003; Burgess et al. 2009; Haisch et al. 2010; Parker & Tinney 2013; Tinney et al. 2005, 2018; Allers & Liu 2020; Jose et al. 2020; Robberto et al. 2020). In late 2016 and early 2017, portions of IC 348 were imaged by the *Hubble Space Telescope* in a medium-band filter aligned with H₂O and CH₄ bands and in two neighboring broad-band filters. In this paper, we present an analysis of those data in order to search for new members of the cluster at planetary masses.

2. WFC3 IMAGING OF IC 348

2.1. Data Collection

IC 348 was observed with the IR channel of *Hubble's* Wide Field Camera 3 (WFC3, Kimble et al. 2008) on several dates between December 2016 and February 2017 through program 14626 (M. Barsony). The camera contains a 1024 × 1024 HgCdTe array in which the pixels have dimensions of $\sim 0''.135 \times 0''.121$. The inner 1014 × 1014 portion of the array detects light, which corresponds to a field of view of $136'' \times 123''$. The observations were performed with the drift-and-shift (DASH) method of imaging multiple fields in a single orbit (Momcheva et al. 2017). After the guide star acquisition for the initial field in a given orbit, re-acquisitions for subsequent fields are omitted and guiding is performed with gyros alone. During the 25 s interval between a pair of non-destructive reads for an exposure, the telescope drift with gyros-only guiding is typically less than half of a WFC3 pixel, so the difference images between adjacent reads can be shifted and combined to produce a single image that has little smearing of the point-spread-function (PSF). For IC 348, the total exposure times were 250 or 275 s for a given field and filter. WFC3 observed 48 fields through three filters, consisting of F125W (1.1–1.4 μm), F139M (1.35–1.41 μm), and F160W (1.4–1.69 μm). In a given orbit, eight fields were imaged in a single filter, so the data were taken across a total of 18 orbits. The WFC3 fields are indicated on a map of the known

¹ Department of Astronomy and Astrophysics, The Pennsylvania State University, University Park, PA 16802; kll207@psu.edu.

² Center for Exoplanets and Habitable Worlds, The Pennsylvania State University, University Park, PA 16802, USA

members of IC 348 in Figure 1 (Luhman et al. 2016; Esplin & Luhman 2017). WFC3 observed the outskirts of the cluster to avoid bright stars, which is recommended with the DASH method (Momcheva et al. 2017). The WFC3 fields encompass 38 of the 480 known members of the cluster.

We note that the relative exposure times among the filters were not optimal for analysis requiring the use of all three filters (e.g., identifying new brown dwarfs). For a given field, the same exposure time was used for each of the three filters. The resulting sensitivity was much lower in F139M than in the other two filters because of its smaller bandpass. Since the F139M images measure molecular absorption from brown dwarfs, they are essential for the photometric identification of brown dwarf candidates, and thus the survey is effectively limited to their (more shallow) depth.

2.2. Data Reduction

We retrieved the raw WFC3/IR images of IC 348 from the Mikulski Archive for Space Telescopes: <https://doi.org/10.17909/t9-d358-qj35>. Each image was split into 25 s difference images using the python routine `wfc3dash`³. The resulting frames were registered and combined using the tasks `tweakreg` and `astrodrizzle` within the DrizzlePac software package. We adopted drop sizes of 1.0 native pixels and a resampled plate scale of $0''.065 \text{ pixel}^{-1}$.

For each reduced image, we used the routine `starfind` in IRAF to identify detected sources and measure their pixel coordinates. We aligned the world coordinate system (WCS) of each F160W image to astrometry of sources in the WFC3 images from Data Release 10 of the United Kingdom Infrared Telescope Infrared Deep Sky Survey (Lawrence et al. 2007). The WCS of each image in the other two filters was aligned to the updated WCS for F160W.

We measured aperture photometry for the sources in the WFC3 images using the IRAF task `phot` with an aperture radius of four pixels and radii of four and eight pixels for the inner and outer boundaries of the sky annulus, respectively. We measured aperture corrections between those apertures and radii of $0''.4$ using bright non-saturated stars. When using gyros-only guiding, the pointing of *Hubble* drifts, and the rate of that drift varies with time. As a result, the sampling of the PSF is not identical among the different fields for a given filter, and hence the aperture corrections can vary among those fields. Therefore, we measured an aperture correction for each image if it contained a sufficient number of bright non-saturated stars. For images with few stars of that kind, we applied the mean aperture correction among all of the images for a given filter that contain bright stars, which corresponded to 0.15, 0.16, and 0.195 mag for F125W, F139M, and F160W, respectively. We applied those corrections and the zero-point Vega magnitudes of 25.1439 (F125W), 23.2093 (F139M), and 24.5037 (F160W) for $0''.4$ apertures⁴ to the photometry. We adopted a minimum error of 0.02 mag for the photometry due to uncertainties in the aperture corrections.

Some of the WFC3 fields overlap (Fig. 1), so we identified detections with matching coordinates among all images in a given filter and computed the mean coordinates and photometry for sources with multiple detections. The resulting catalogs for the three filters were then matched to each other to form a single catalog for the entire set of images. That catalog contains 1552 sources with non-saturated detections in all three bands.

3. IDENTIFICATION OF BROWN DWARF CANDIDATES

The F139M filter of WFC3 is centered on absorption bands from H₂O and CH₄ while F125W and F160W encompass continuum at shorter and longer wavelengths. As a result, objects with strong absorption in those bands will exhibit blue colors in $m_{125} - m_{139}$ and red colors in $m_{139} - m_{160}$, which should be distinctive from most other astronomical sources. To use those colors to identify candidate brown dwarfs in IC 348, we have plotted a diagram of $m_{139} - m_{160}$ versus $m_{125} - m_{139}$ in Figure 2 for all sources from the WFC3 images that have photometric errors less than 0.1 mag in each of three bands. Since the WFC3 images are deeper in F125W and F160W than in F139M (Section 2.1), that sample is effectively limited by the sensitivity in F139M and all of the selected sources have small errors in F125W and F160W (no larger than 0.02 mag). To further refine our selection of brown dwarf candidates, we have included in Figure 2 a diagram of $z' - m_{125}$ versus $m_{125} - m_{139}$ in which the z' data were measured by Luhman et al. (2016) using deep imaging from Alves de Oliveira et al. (2013). We also show m_{160} versus $m_{125} - m_{139}$ to illustrate the range of magnitudes spanned by any candidates that we identify. In each of the three diagrams in Figure 2, a reddening vector for $A_K = 0-1$ is shown for the extinction curve from Schlafly et al. (2016).

In Figure 2, we have indicated the known members of IC 348 that are within the WFC3 images and are not saturated. The members earlier and later than M8 are shown with different symbols. A spectral type of M8 is predicted to correspond to a mass of $\sim 30 M_{\text{Jup}}$ for ages of a few Myr (Baraffe et al. 1998). As expected, the late-type members are blue in $m_{125} - m_{139}$ and red in $m_{139} - m_{160}$, making them distinctive from most other sources in the WFC3 images. To identify brown dwarf candidates based on colors of that kind, the reddening vector in the diagram of $m_{139} - m_{160}$ versus $m_{125} - m_{139}$ has been placed along the lower envelope of the known members later than M8. Twelve candidates appear above that vector, which are marked with open circles and triangles according to whether we have observed them with spectroscopy (Section 4). Six of the candidates have detections in z' , so they appear in the diagram in Figure 2 that contains $z' - m_{125}$. Four of those six candidates have similar positions in that diagram as the known late-type members, which supports their candidacy as cool objects. The other two candidates (LRL 60032 and LRL 91235) are somewhat bluer in $z' - m_{125}$ than the known $>M8$ members. Nine of the 12 candidates have detections in images at J , H , and K_s from Luhman et al. (2016), so we have plotted them in a diagram of $J - H$ versus $H - K_s$ in Figure 3 with all known members of IC 348. Five of those candidates (the four with spectroscopy and LRL 61451) have colors similar to those of the known $>M8$ members. Two candidates, LRL 60032 and LRL 60101,

³ <https://github.com/gbrammer/wfc3dash>

⁴ <https://www.stsci.edu/hst/instrumentation/wfc3/data-analysis/photometric-calibrations>

depart modestly from the known members in those colors. The two remaining candidates, LRL 52142 and LRL 60203, are significantly redder in $J-H$ than known late-type members near the same $H-K_s$.

In the diagram of m_{160} versus $m_{125} - m_{139}$ in Figure 2, the 12 brown dwarf candidates range from $m_{160} \sim 18-21$ and are fainter than most of the known members of IC 348 that are within the WFC3 images. We compare 11 of the 12 candidates to all known members of the cluster in a diagram of K_s versus $H - K_s$ in Figure 3. One of the candidates, LRL 91235, lacks photometry in those bands. Most of the candidates are fainter than the known members in K_s , although correcting the photometry for extinction would likely increase the overlap between the candidates and known members. If the candidates are dereddened to the intrinsic colors of the known late-type members (e.g., $m_{125} - m_{139} \sim 0$), roughly half of the candidates would be fainter than the known members in terms of extinction-corrected magnitudes.

We present the sample of 12 brown dwarf candidates in Table 1, which includes coordinate-based designations, the photometry that we measured from the WFC3 images, and photometry in JHK_s from Luhman et al. (2016).

4. SPECTROSCOPY OF BROWN DWARF CANDIDATES

We have performed near-IR spectroscopy on the four brightest brown dwarf candidates from the WFC3 images to measure their spectral types and check for evidence of youth, which would support their membership in IC 348. The spectra were obtained with the Gemini Near-Infrared Spectrograph (GNIRS, Elias et al. 2006) during nights in February and March of 2020. The instrument was operated in the cross-dispersed mode with the $1''$ slit and the 31.7 l mm^{-1} grating. That configuration provided a resolution of ~ 600 and a wavelength coverage of $0.8-2.5 \mu\text{m}$. For each target, the slit was rotated to the parallactic angle and exposures were taken at two positions along the slit separated by $3''$ in an ABBA pattern. The numbers of exposures and exposure times ranged from $8 \times 180 \text{ sec}$ to $12 \times 250 \text{ sec}$. The spectra were reduced and corrected for telluric absorption with routines in IRAF. The reduced spectra of the four candidates are presented in Figure 4. The spectra have been binned to a resolution of ~ 100 to improve their signal-to-noise ratios (S/N's). The unbinned spectra are provided in an electronic file that accompanies Figure 4.

In Figure 4, we have included the spectra of a young L dwarf standard from Luhman et al. (2017) and a field L dwarf standard, 2MASS J11463449+2230527 (L2V, Kirkpatrick et al. 1999). Like those L dwarfs, the four brown dwarf candidates exhibit strong absorption bands from H_2O , which confirms their cool nature. The shape of the H -band continuum is sensitive to surface gravity and hence age (Lucas et al. 2001), as illustrated with the young and field L dwarf standards in Figure 4. LRL 40013 and LRL 52749 have triangular H -band continua, indicating that they are young, although the S/N for the latter is low enough that we treat its age classification as tentative. The S/N's of the spectra for LRL 60119 and LRL21460 are too low for definitive age classifications based on that feature, although the latter may have the H -band plateau found in field L dwarfs. We have measured spectral types and reddenings from the spectra

of the four candidates through comparison to the young standard spectra from Luhman et al. (2017). Those classifications are listed in Table 1. If any candidate is a field dwarf rather than young object, then it should be classified through a comparison to a field standard, which would likely result in a different spectral type.

5. DISCUSSION

Through spectroscopy, we have demonstrated that four of the 12 brown dwarf candidates in IC 348 have late spectral types, two of which appear to be young, and hence are likely to be members of the cluster. The spectra of the other two candidates have insufficient S/N's for assessments of their ages and cluster membership. One of the candidates classified as young, LRL 52749, is the faintest known member (by a very small margin) in extinction-corrected K_s . We have estimated a mass of $4-5 M_{\text{Jup}}$ for that object from a comparison of the luminosities predicted by evolutionary models at an age of 3 Myr (Chabrier et al. 2000; Baraffe et al. 2015) to the value derived by combining its K_s photometry with a K -band bolometric correction for young L dwarfs (Filippazzo et al. 2015) and the distance of IC 348 (321 pc, Ortiz-León et al. 2018).

Among the remaining eight objects that lack spectroscopy, LRL 61451 is the most promising candidate for a late-type object based on its $J-H$ and $H-K_s$ colors (Section 3, Fig. 3). If it is a member, it could be the faintest known member in extinction-corrected photometry. The near-IR colors of LRL 60032 and LRL 60101 are close enough to those of known late-type members of IC 348 that we consider them to be viable candidates. LRL 52542 has the reddest $H-K_s$ among the 11 candidates with measurements of that color (Fig. 3), but it is only moderately red in $m_{125} - m_{139}$. The combination of those two colors suggests that LRL 52542 is a highly reddened brown dwarf. If its position in the diagram of K_s versus $H - K_s$ in Figure 3 is dereddened to the sequence of lightly reddened members, it would have $A_K \sim 1.6$ and $K_s \sim 16.2$. LRL 60203, LRL 52142, and LRL 91235 are less likely to have late spectral types based on $z' - m_{125}$ or JHK_s colors (Section 3). The last remaining candidate, LRL 61953, has too little photometry beyond the WFC3 bands (only H and K_s) for further assessing whether it might have a late spectral type.

We can examine the implications of our sample of brown dwarf candidates for the initial mass function (IMF) in IC 348. Since the positions of the WFC3 fields were selected to avoid brighter stars, the sample of cluster members within those fields is biased against more massive stars. For instance, the earliest known members within the WFC3 images have spectral types of M4 ($\sim 0.3 M_{\odot}$). As a result, the WFC3 fields cannot be used to construct an IMF that is representative of the cluster's stellar population for the full range of masses. Therefore, we can characterize the IMF only at lower masses in the WFC3 fields.

The current census of members of IC 348 is nearly complete for $K_s < 16.8$ at $A_J < 1.5$ ($A_K < 0.6$) in an area that encompasses most of the WFC3 images (Luhman et al. 2016), so we consider members and candidates within that extinction limit for the IMF sample in the WFC3 fields. That criterion is satisfied by 22 of the 38 known members that are within the WFC3 im-

ages and eight of the 12 WFC3 candidates. The four candidates that appear to have $A_K > 0.6$ based on their colors consist of LRL 52142, LRL 52542, LRL 61953, and LRL 60203. As done in some of our previous studies of the IMF in IC 348 and other young clusters (Luhman et al. 2016), we use a distribution of extinction-corrected near-IR magnitudes as an observational proxy for the IMF. In Figure 5, we show the distributions of extinction-corrected magnitudes in either H or m_{160} for the 22 known members of IC 348 that are within the WFC3 images and have $A_K < 0.6$ and the eight WFC3 candidates that appear to have $A_K < 0.6$. The extinctions for the known members are from Luhman et al. (2016) and the extinctions for the candidates are estimated from $m_{125} - m_{139}$ assuming an intrinsic value similar to that of the known late-type members. We use measurements of m_{160} in the distributions when they are available and otherwise use H for stars that saturated in F160W. The median value of $m_{160} - H$ is ~ 0.31 for late-type members of IC 348, so the two bands are sufficiently similar that they can be shown together in the distributions for Figure 5.

To interpret the distributions in Figure 5 in terms of a mass function, we have marked the magnitudes that are predicted to correspond to $0.1 M_\odot$, $10 M_{\text{Jup}}$, and $3 M_{\text{Jup}}$ for an age of 3 Myr according to evolutionary models (Chabrier et al. 2000; Baraffe et al. 2015). Based on those theoretical magnitudes, Figure 5 contains 13 objects between $0.1 M_\odot$ and $10 M_{\text{Jup}}$, all of which are known members. If the substellar mass function is flat in logarithmic units ($dN/d\log M \propto M^{-\Gamma}$ where $\Gamma = 0$), the mass interval from 3–10 M_{Jup} would contain ~ 6.5 objects. The distributions in Figure 5 contain four known members and seven candidates in the magnitude range corresponding to 3–10 M_{Jup} , and two of those candidates have been classified as members through our spectroscopy. Thus, the mass function in the WFC3 fields is consistent with $\Gamma \gtrsim 0$, although the uncertainties in the slope are large given the small numbers of objects in question and the unknown membership status of some of the candidates. Constraints on the mass function at planetary masses in IC 348 would be improved through spectroscopy of the remaining candidates and a survey of areas of the cluster that contain larger numbers of members.

This work was supported by NASA grant 80NSSC18K0444 and is based on observations made with the NASA/ESA *Hubble Space Telescope* obtained at the Space Telescope Science Institute, which is operated by the Association of Universities for Research in Astronomy, Inc., under NASA contract NAS 5-26555. These observations are associated with program 14626. The Gemini data were obtained through program GN-2020A-FT-102. Gemini Observatory is operated by AURA under a cooperative agreement with the NSF on behalf of the Gemini partnership: the NSF (United States), the NRC (Canada), CONICYT (Chile), the ARC (Australia), Ministério da Ciência, Tecnologia e Inovação (Brazil) and Ministerio de Ciencia, Tecnología e Innovación Productiva (Argentina). The Center for Exoplanets and Habitable Worlds is supported by the Pennsylvania State University, the Eberly College of

Science, and the Pennsylvania Space Grant Consortium.

REFERENCES

- Allers, K. N., & Liu, M. C. 2020, *ApJ*, submitted
- Alves de Oliveira, C., Moraux, E., Bouvier, J., et al. 2013, *A&A*, 549, A123
- Baraffe, I., Chabrier, G., Allard, F., & Hauschildt, P. H. 1998, *A&A*, 337, 403
- Baraffe, I., Horneier, D., Allard, F., & Chabrier, G. 2015, *A&A*, 577, 42
- Bardalez Gagliuffi, D. C., Faherty, J. K., Schneider, A. C., et al. 2020, *ApJ*, in press
- Bell, C. P. M., Naylor, T., Mayne, N. J., Jeffries, R. D., & Littlefair, S. P. 2013, *MNRAS*, 434, 806
- Best, W. M. J., Liu, M. C., Dupuy, T. J., & Magnier, E. A. 2017, *ApJ*, 843, L4
- Burgasser, A. J., Lopez, M. A., Mamajek, E. E., et al. 2016, *ApJ*, 820, 32
- Burgess, A. S. M., Moraux, E., Bouvier, J., et al. 2009, *A&A*, 508, 823
- Chabrier, G., Baraffe, I., Allard, F., & Hauschildt, P. 2000, *ApJ*, 542, 464
- Cushing, M. C., Kirkpatrick, J. D., Gelino, C. R., et al. 2011, *ApJ*, 743, 50
- Elias, J. H., Joyce, R. R., Liang, M., et al. 2006, *Proc. SPIE*, 6269, 62694C
- Esplin, T. L., & Luhman, K. L. 2017, *AJ*, 154, 134
- Esplin, T. L., & Luhman, K. L. 2019, *AJ*, 158, 54
- Esplin, T. L., Luhman, K. L., Faherty, J. K., Mamajek, E. E., & Bochanski, J. J. 2017, *AJ*, 154, 46
- Filippazzo, J. C., Rice, E. L., Faherty, J., et al. 2015, *ApJ*, 810, 158
- Gagné, J., Allers, K. N., Theissen, C. A., et al. 2018, *ApJ*, 854, L27
- Haisch, K. E., Barsony, M., & Tinney, C. 2010, *ApJ*, 719, 90
- Herbst, W. 2008, in *Handbook of Star Forming Regions, Vol. 1, The Northern Sky*, ASP Monograph Series 4, ed. B. Reipurth (San Francisco, CA: ASP), 372
- Jose, J., Biller, B. A., Albert, L., et al. 2020, *ApJ*, 892, 122
- Kellogg, K., Metchev, S., Geißler, K., et al. 2015, *AJ*, 150, 182
- Kimble, R. A., MacKenty, J. W., O'Connell, R. W., & Townsend, J. A. 2008, *Proc. SPIE*, 7010, 43
- Kirkpatrick, J. D., Martin, E. C., Smart, R. L., et al. 2019, *ApJS*, 240, 19
- Kirkpatrick, J. D., Reid, I. N., Liebert, J., et al. 1999, *ApJ*, 519, 802
- Lawrence, A., Warren, S. J., Almaini, O., et al. 2007, *MNRAS*, 379, 1599
- Liu, M. C., Magnier, E. A., Deacon, N. R., et al. 2013, *ApJ*, 777, L20
- Lodieu, N., Zapatero Osorio, M. R., Béjar, V. J. S., & Peña Ramírez, K. 2018, *MNRAS*, 473, 2020
- Lucas, P. W., Roche, P. F., Allard, F., & Hauschildt, P. H. 2001, *MNRAS*, 326, 695
- Luhman, K. L. 2014, *ApJ*, 786, L18
- Luhman, K. L., Esplin, T. E., & Loutrel, N. P. 2016, *ApJ*, 827, 52
- Luhman, K. L., Mamajek, E. E., Shukla, S. J., & Loutrel, N. P. 2017, *AJ*, 153, 46
- Luhman, K. L., Rieke, G. H., Lada, C. J., & Lada, E. A. 1998, *ApJ*, 508, 347
- Luhman, K. L., Stauffer, J. R., Muench, A. A., et al. 2003, *ApJ*, 593, 1093
- Mainzer, A. K., & McLean, I. S. 2003, *ApJ*, 597, 555
- Meisner, A. M., Caselden, D., Kirkpatrick, J. D., et al. 2020, *ApJ*, 889, 74
- Momcheva, I. G., van Dokkum, P. G., van der Wel, A., et al. 2017, *PASP*, 129, 015004
- Najita, J., Tiede, G. P., & Carr, J. S. 2000, *ApJ*, 541, 977
- Ortiz-León, G. N., Loinard, L., Dzib, S. A., et al. 2018, *ApJ*, 865, 73
- Parker, S. R., & Tinney, C. G. 2013, *MNRAS*, 430, 1208
- Robberto, M., Gennaro, M., Giulia Ubeira Gabellini, M., et al. 2020, *ApJ*, in press
- Schlafly, E. F., Meisner, A. M., Stutz, A. M., et al. 2016, *ApJ*, 821, 78
- Schneider, A. C., Windsor, J., Cushing, M. C., Kirkpatrick, J. D., & Wright, E. L. 2016, *ApJ*, 822, L1
- Scholz, A., Jayawardhana, R., Muzic, K., et al. 2012, *ApJ*, 756, 24
- Tinney, C. G., Burgasser, A. J., Kirkpatrick, J. D., McElwain, M. W. 2005, *AJ*, 130, 2326
- Tinney, C. G., Kirkpatrick, J. D., Faherty, J. K., et al. 2018, *ApJS*, 236, 28
- Zapatero Osorio, M. R., Béjar, V. J. S., & Peña Ramírez, K. 2017, *ApJ*, 842, 65

TABLE 1
CANDIDATE MEMBERS OF IC 348

IC 348 IRS	LRL ^a	Spectral Type/ A_K	Young?	m_{125} (mag)	m_{139} (mag)	m_{160} (mag)	J (mag)	H (mag)	K_s (mag)
J03433364+3201037	61953	...	?	22.13±0.03	21.53±0.09	20.38±0.02	...	19.98±0.10	18.78±0.06
J03433755+3201489	21460	M9-L2/0.15	N?	19.87±0.02	19.91±0.02	19.13±0.02	19.80±0.02	18.87±0.04	18.07±0.03
J03433807+3208133	60101	...	?	21.19±0.02	21.02±0.05	20.15±0.02	21.15±0.09	19.68±0.07	18.79±0.04
J03433941+3208131	60032	...	?	20.80±0.02	20.75±0.04	20.05±0.02	20.80±0.05	20.00±0.12	19.09±0.05
J03434218+3212130	91235	...	?	21.62±0.02	21.62±0.08	20.94±0.02
J03434453+3209113	60119	L0-L4/0.20	?	20.56±0.02	20.50±0.03	19.60±0.02	20.57±0.03	19.29±0.03	18.29±0.02
J03435236+3158556	61451	...	?	21.02±0.02	20.99±0.04	20.03±0.02	20.91±0.09	19.60±0.06	18.60±0.02
J03441321+3200588	52542	...	?	21.46±0.02	21.29±0.07	19.84±0.02	...	19.30±0.05	17.80±0.02
J03442211+3214105	40013	M9.5-L2/0.10	Y	18.82±0.02	18.95±0.02	18.12±0.02	18.77±0.02	17.77±0.02	16.98±0.02
J03443946+3156549	60203	...	?	21.40±0.02	20.86±0.03	19.71±0.02	21.33±0.08	19.33±0.03	18.40±0.03
J03444366+3158452	52142	...	?	21.55±0.02	21.23±0.05	19.97±0.02	21.66±0.12	19.76±0.05	18.62±0.02
J03445439+3209485	52749	L0-L4/0.10	Y?	20.57±0.02	20.38±0.04	19.57±0.02	20.30±0.02	19.18±0.03	18.25±0.02

^a These source names are a continuation of the designation numbers from Luhman et al. (1998).

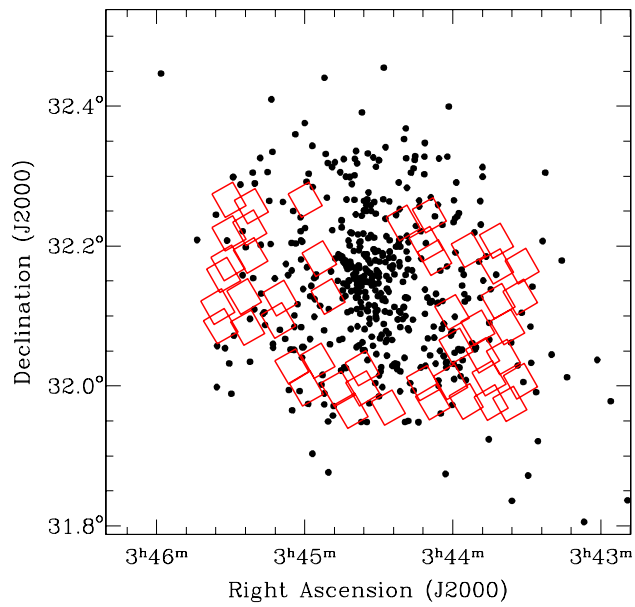


FIG. 1.— Map of the known members of IC 348 (Luhman et al. 2016; Esplin & Luhman 2017) and the fields imaged by WFC3 in this study.

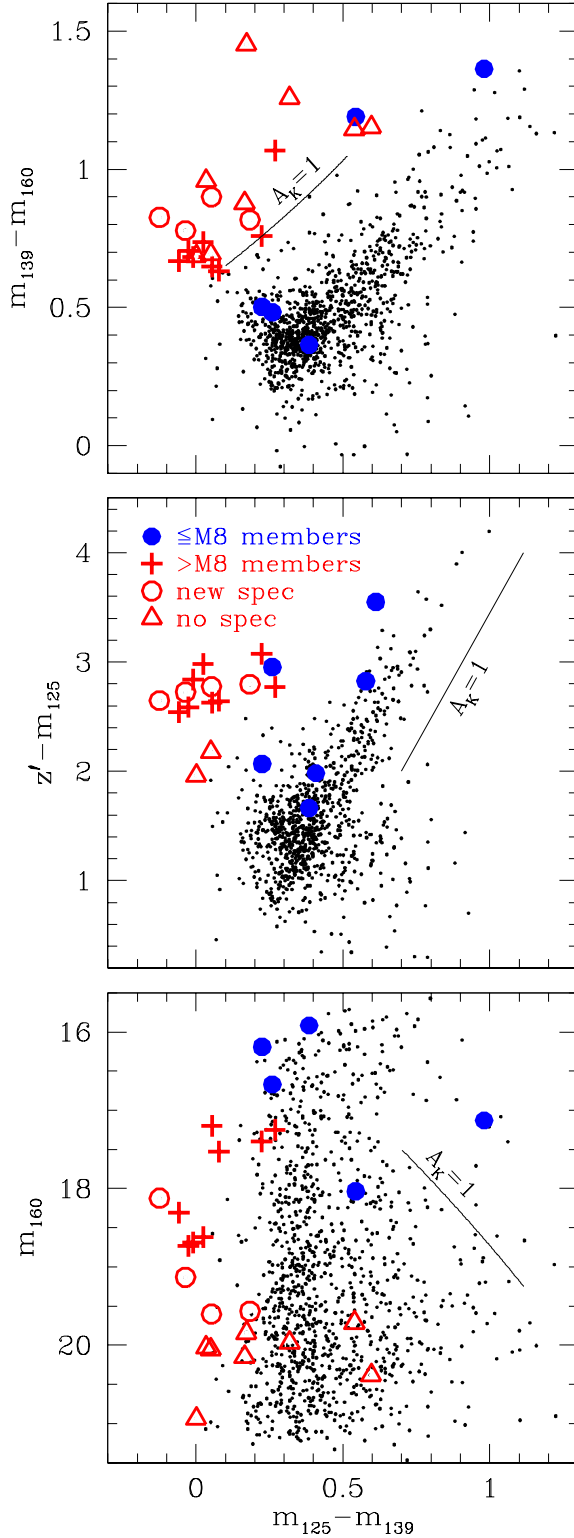


FIG. 2.— Color-color and color-magnitude diagrams for fields in IC 348 that were imaged by WFC3, which are constructed from three WFC3 bands and ground-based photometry in z' . We have marked previously known members of IC 348 that are within the WFC3 images and are not saturated (filled circles for $\leq M8$ and crosses for $> M8$). The $> M8$ members have distinctive positions in the two color-color diagrams relative to most other stars. A reddening vector has been placed near the lower envelope of the $> M8$ members in the top diagram. We have selected candidates for new late-type members of IC 348 based on positions above that vector (Table 1). Four of the resulting candidates have new spectroscopy (open circles, Fig. 4) while the remaining candidates lack spectra (open triangles). Nearly all of the sources that are not labeled as known or candidate members of IC 348 are expected to be field stars and galaxies (small points).

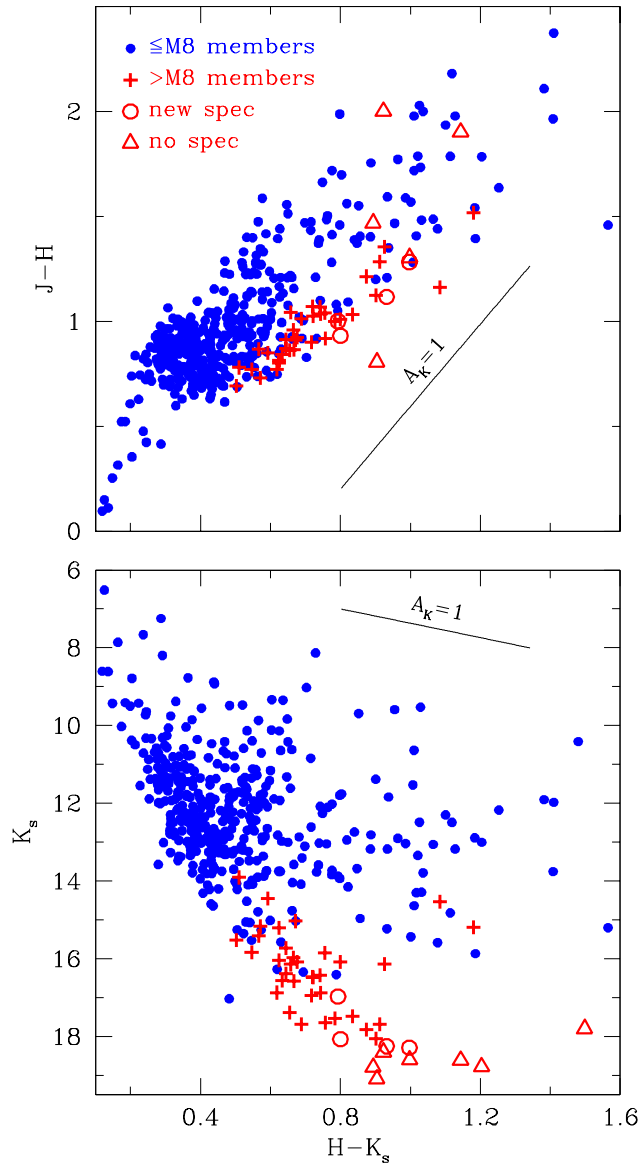


FIG. 3.— Color-color and color-magnitude diagrams for known members of IC 348 with spectral types of $\leq M8$ and $>M8$ (filled circles and crosses) and candidate members selected from Figure 2 (Table 1) that have new spectroscopy (open circles, Fig. 4) and that lack spectra (open triangles).

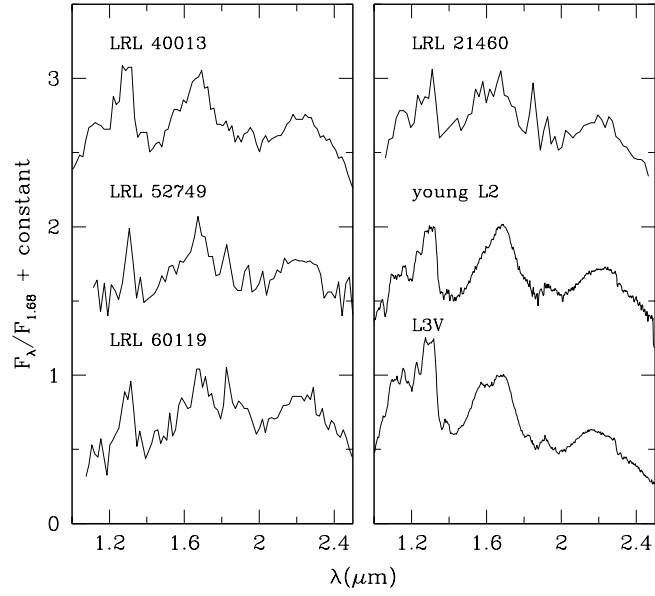


FIG. 4.— Near-IR spectra of four candidate substellar members of IC 348 selected from Figure 2 (LRL designations), the young L2 standard spectrum from Luhman et al. (2017), and a field L dwarf (2MASS J11463449+2230527). These data are displayed at a resolution of ~ 100 . The data used to create this figure are available.

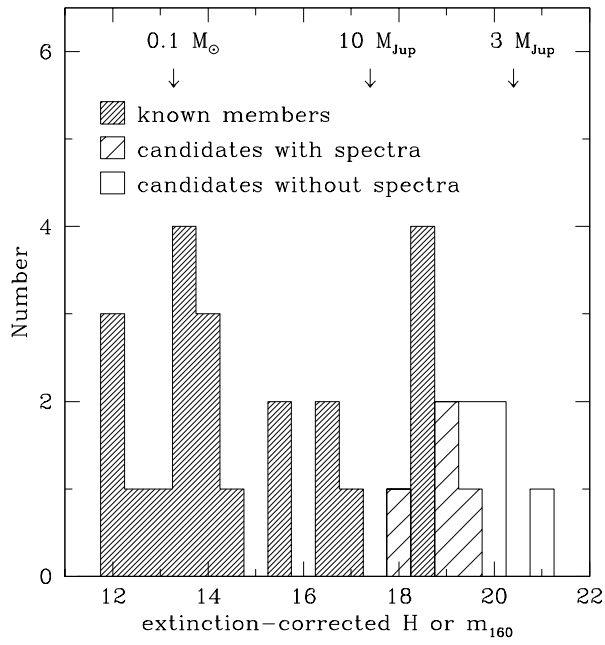


FIG. 5.— Distributions of extinction-corrected H or m_{160} for previously known members of IC 348 that are within the WFC3 fields and have $A_K < 0.6$ (finely shaded histogram) and WFC3 candidates from Figure 2 that have $A_K < 0.6$. The candidates are divided into those that have been observed spectroscopically (coarsely shaded histogram, Fig. 4) and those that lack spectra (open histogram). We have indicated the magnitudes that correspond to $0.1 M_{\odot}$, $10 M_{\text{Jup}}$, and $3 M_{\text{Jup}}$ for an age of 3 Myr according to evolutionary models (Chabrier et al. 2000; Baraffe et al. 2015).